Naval Research Laboratory
Washington, DC 20375-5320

Ground State Resonance Structure Calculated by Density Functional Theory for Estimating the Dielectric Response of Some Typical High Explosives

A. Shabaev

George Mason University
Fairfax, Virginia

S.G. Lambrakos
N. Bernstein
V. Jacobs

Center for Computational Materials Science
Materials Science and Technology Division

D. Finkenstadt

U.S. Naval Academy
Annapolis, Maryland

December 30, 2010

REPORT DOCUMENTATION PAGE

1. REPORT DATE (DD-MM-YYYY)	2. REPORT TYPE	3. DATES COVERED (From - To)
30-12-2010	NRL Memorandum Report	01-10-2009 to 30-09-2010

4. TITLE AND SUBTITLE

Ground State Resonance Structure Calculated by Density Functional Theory for Estimating the Dielectric Response of Some Typical High Explosives

5a. CONTRACT NUMBER

5b. GRANT NUMBER

5c. PROGRAM ELEMENT NUMBER

6. AUTHOR(S)

A. Shabaev,* S.G. Lambrakos, N. Bernstein, V. Jacobs, and D. Finkenstadt†

5d. PROJECT NUMBER

5e. TASK NUMBER

5f. WORK UNIT NUMBER
9191

7. PERFORMING ORGANIZATION NAME(S) AND ADDRESS(ES)

Naval Research Laboratory, Code 6394
4555 Overlook Avenue, SW
Washington, DC 20375-5320

8. PERFORMING ORGANIZATION REPORT NUMBER

NRL/MR/6390--10-9307

9. SPONSORING / MONITORING AGENCY NAME(S) AND ADDRESS(ES)

Office of Naval Research
One Liberty Center
875 North Randolph Street, Suite 1425
Arlington, VA 22203-1995

10. SPONSOR / MONITOR'S ACRONYM(S)

ONR

11. SPONSOR / MONITOR'S REPORT NUMBER(S)

12. DISTRIBUTION / AVAILABILITY STATEMENT

Approved for public release; distribution is unlimited.

13. SUPPLEMENTARY NOTES

*George Mason University, Department of Computation and Data Sciences, Fairfax, VA 22030
†U.S. Naval Academy, Physics Department, Annapolis, MD 21402

14. ABSTRACT

We present calculations of ground state resonance structure associated with the high explosives B-HMX, PETN, RDX, TNT1 and TNT2 using density functional theory (DFT), which is for the construction of parameterized dielectric response functions for excitation by electromagnetic waves at compatible frequencies. These dielectric functions provide for different types of analyses concerning the dielectric response of explosives. In particular, these dielectric response functions provide quantitative initial estimates of spectral response features for subsequent adjustment with respect to additional information such as laboratory measurements and other types of theory based calculations. With respect to qualitative analysis, these spectra provide for the molecular level interpretation of response structure. The DFT software NRLMOL was used for the calculations of ground state resonance structure presented here.

15. SUBJECT TERMS

Density functional theory (DFT)   Explosives
Dielectric functions

16. SECURITY CLASSIFICATION OF:			17. LIMITATION OF ABSTRACT	18. NUMBER OF PAGES	19a. NAME OF RESPONSIBLE PERSON
a. REPORT	**b. ABSTRACT**	**c. THIS PAGE**	UL	32	Samuel G. Lambrakos
Unclassified	Unclassified	Unclassified			**19b. TELEPHONE NUMBER** (include area code) (202) 767-2601

Standard Form 298 (Rev. 8-98)
Prescribed by ANSI Std. Z39.18

Contents

"

Ground State Resonance Structure Calculated by Density Functional Theory For Estimating the Dielectric Response of Some Typical High Explosives

Introduction

A significant aspect of using response spectra calculated by density functional theory, DFT, for the direct construction of permittivity functions is that it adopts the perspective of computational physics, according to which a numerical simulation represents another source of "experimental" data. This perspective is significant in that a general procedure may be developed for construction of permittivity functions using DFT calculations as a quantitative initial estimate of spectral response features for subsequent adjustment with respect to additional information such as experimental measurements and other types of theory based calculations. That is to say, for the purpose of simulating many electromagnetic response characteristics of materials, DFT is sufficiently mature for the purpose of generating data complementing, as well as superseding, experimental measurements.

In the case of THz excitation of materials, the procedure of using response spectra calculated using DFT for the direct construction of permittivity functions is well posed owing to the physical characteristic of THz excitation. In particular, it is important to note that the procedure for constructing a permittivity function using response spectra calculated using DFT is physically consistent with the characteristically linear response associated with THz excitation of molecules. Accordingly, one observes a correlation between the advantages of using THz excitation for detection of IEDs (and ambient materials) and those for its numerical simulation based on DFT. Specifically, THz excitation is associated with frequencies that are characteristically perturbative to molecular states, in contrast to frequencies that can induce appreciable electronic state transitions. Of course, the practical aspect of the perturbative character of THz excitation for detection is that detection methodologies can be developed which do not damage materials under examination. The perturbative character of THz excitation with respect to molecular states has significant implications with respect to its numerical simulation based on DFT. It follows then that, owing to the perturbative character of THz excitation, which is characteristically linear, one is able to make a direct association between local oscillations about ground-state minima of a given molecule and THz excitation spectra.

In what follows, calculations are presented of ground state resonance structure associated with the high explosives β–HMX, PETN, RDX, TNT1 and TNT2 using DFT. This resonant structure is for the construction of parameterized dielectric response functions for excitation by electromagnetic waves at compatible frequencies. For this purpose the DFT software NRLMOL was adopted [4-10].

The organization of the subject areas presented here are as follows. First, a general review of the elements of DFT relevant for the calculation of absorption spectra is presented. This review focuses on the specific numerical implementation of DFT, which is embodied by the NRLMOL software. Second, a general review is presented concerning the formal structure of permittivity functions in terms of analytic function representations. An understanding of the formal structure of permittivity functions in terms of both physical consistency and causality is important for post-processing of DFT calculations for the purpose of constructing permittivity functions. Third, information concerning the ground state resonance structure of the explosives β–HMX, PETN, RDX, TNT1 and TNT2, which is obtained using DFT, is presented as a set of case studies. This information consists of the ground state molecular geometry and response spectrum for an isolated molecule. In addition, for each of the explosives, a prototype calculation is presented to demonstrate the construction of parameterized permittivity functions using response spectra calculated using DFT. Fourth, a discussion is presented that elucidates the utility of the information concerning the ground state resonance structure of the explosives considered. This discussion also indicates the relevance of this information for the

1

construction of permittivity functions for frequencies that exceed the THz regime. Finally, a conclusion is given, indicating possible future pathways for extension of the methodology presented and the calculation of spectra for other molecular systems.

Construction of Permittivity Functions using DFT

Density Functional Theory

The application of density functional theory (DFT) and related methodologies for the determination of electromagnetic response characteristics is important for the analyses of parameter sensitivity. That is to say, many characteristics of the electromagnetic response of a given material may not be detectable, or in general, not relevant for detection. Accordingly, sensitivity analyses concerning the electromagnetic response of layered composite systems can incorporate the results of simulations using DFT, and related methodologies, to provide realistic limits on detectability that are independent of a specific system design for IED detection. In addition, analysis of parameter sensitivity based on atomistic response characteristics of a given material, obtained by DFT, provide for an "optimal" best fit of experimental measurements for the construction of permittivity functions. It follows that within the context of parameter sensitivity analysis, data obtained by means of DFT represents a true complement to data that has been obtained by means of experimental measurements.

The NRLMOL software can be used to compute an approximation of the IR absoprtion spectrum of a molecule [4-10]. NRLMOL uses density functional theory to compute the ground state electronic structure in the Born-Oppenheimer approximation using Kohn-Sham density functional theory [2]. NRLMOL uses a Gaussian orbital basis to describe the electronic wavefunctions and density, with numerical integration that is nearly exact to machine precision. For a given set of nuclear positions, the calculation directly gives the electronic charge density of the molecule, the total energy E, and the forces on each atom

$$F_\alpha^i = \frac{\partial E}{\partial r_\alpha^i} \tag{1}$$

where r_α^i is the α cartesian component of the position of atom i, and F_α^i is the corresponding force. The dipole moment of the molecule is easily computed from the combined (nuclear and electronic) charge density.

To compute the miminum energy atomic configuration, NRLMOL uses the conjugate-gradient algorithm [11]. The vibrational spectrum depends on the atomic mass matrix $M_{i\alpha j\beta} = \delta_{ij}\delta_{\alpha\beta}m_i$ where m_i is the mass of atom i, and the energy second derivative matrix

$$D_{i\alpha j\beta} = \frac{\partial^2 E}{\partial r_\alpha^i \partial r_\beta^j} \tag{2}$$

through the eigenproblem

$$\sum_{j\beta}\left(D_{i\alpha j\beta} - \varepsilon_n M_{i\alpha j\beta}\right)X_{j\beta}^{(n)} = 0. \tag{3}$$

The generalized eigenvalues ε_n are the squares of the vibrational frequencies $\omega_n = 2\pi c v_n$, and the eigenvectors $X_{j\beta}^{(n)}$ give the corresponding atomic displacements:

2

$$\Delta r_{j\beta} = \sum_n Q_n \cdot X_{j\beta}^{(n)} \tag{4}$$

where Q_n is the normal mode coordinate. The eigenvectors are normalized according to the condition

$$\sum_{i\alpha, j\beta} X_{i\alpha}^{(m)} M_{i\alpha j\beta} X_{j\beta}^{(n)} = \delta_{mn}. \tag{5}$$

NRLMOL computes the energy second derivatives Eq.(2) by finite differences, computing the forces for displacement perturbations of each atom along each Cartesian direction. The first derivatives of the dipole moment with respect to atomic positions $\partial \vec{\mu} / \partial r_\alpha^i$ are also computed at the same time. Each vibrational eigenmode leads to one peak in the absorption spectrum, at a frequency equal to the mode's eigenfrequency. It is significant to note, however, that the finite-difference energy second derivatives represent an approximation of the exact second derivatives and a correction that reduces the associated error of this approximation is obtained by directly recomputing the second derivatives of the energy with respect to the eigenvectors displacements.

The absorption intensity corresponding to a particular eigenmode for a single molecule is given by

$$I_n = \frac{\pi}{3c} \left| \frac{d\vec{\mu}}{dQ_n} \right|^2, \tag{6}$$

where c is the speed of light in a vacuum, and

$$\frac{d\vec{\mu}}{dQ_n} = \sum_{\alpha i} \frac{\partial \vec{\mu}}{\partial r_\alpha^i} X_{i\alpha}^{(n)}. \tag{7}$$

The intensity Eq.(6) must then be multiplied by the number density of molecules to give an absorption strength. It follows that the absorption spectrum calculated by NRLMOL is a sum of delta functions whose positions and magnitudes correspond to the vibrational frequencies and magnitudes, respectively. In principle, however, these spectral components must be broadened and shifted to account for anharmonic effects such as finite mode lifetimes and inter-mode couplings.

Remark. The ground state resonance modes calculated by NRLMOL, which are commensurate with electromagnetic wave excitation at THz frequencies, follow a "frozen phonon" type method [12]. This method entails numerically a predictor-corrector procedure.

Dielectric Permittivity Functions

The general approach of constructing permittivity functions according to the best fit of available data for given material corresponding to many different types of experimental measurements is not unprecedented and has been typically the dominant approach, e.g., the permittivity function of water. The general simulation framework presented here considers an extension of this approach in that calculations of electromagnetic response based on DFT are incorporated as data for construction of permittivity functions. The inclusion of this type of information is essential for accessing what spectral response features at the molecular level are actually detectable with respect to a given set of detection parameters. Accordingly, permittivity functions having been constructed using DFT calculations provide a quantitative correlation between macroscopic material response and molecular structure. Within this context it is not important that the permittivity function be quantitatively accurate for the

3

purpose of being adopted as input for system simulation. Rather, it is important that the permittivity function be qualitatively accurate in terms of specific dielectric response features for the purpose of sensitivity analysis, which is relevant for the assessment of absolute detectability of different types of molecular structure with respect to a given set of detection parameters. That is to say, permittivity functions that have been determined using DFT can provide a mechanistic interpretation of material response to electromagnetic excitation that could establish the reliability of a given detection methodology for detection of specific molecular characteristics. Within the context of practical application, permittivity functions having been constructed according to the best fit of available data would be "correlated" with those obtained using DFT for proper interpretation of permittivity-function features. Subsequent to establishment of good correlation between DFT and experiment, DFT calculations can be adopted as constraints for the purpose of constructing permittivity functions, whose features are consistent with molecular level response, for adjustment relative to specific sets of either experimental data or additional molecular level information.

The construction of permittivity functions using DFT calculations involves, however, an aspect that requires serious consideration. This aspect concerns the fact that a specific parametric function representation must be adopted. Accordingly, any parametric representation, i.e., parameterization, adopted for permittivity-function construction must be physically consistent with specific molecular response characteristics, while limiting the inclusion of feature characteristics that tend to mask response signatures that may be potentially detectable.

In principle, parameterizations are of two classes. One class consists of parameterizations that are directly related to molecular response characteristics. This class of parameterizations would include spectral scaling and width coefficients. The other class consists of parameterizations that are purely phenomenological and are structured for optimal and convenient best fits to experimental measurements. A sufficiently general parameterization of permittivity functions is given by Drude-Lorentz approximation [13]

$$\varepsilon(\nu) = \varepsilon'(\nu) + i\varepsilon''(\nu) = \varepsilon_\infty + \sum_{n=1}^{N} \frac{\nu_{np}^2}{(\nu_{no}^2 - \nu^2) - i\gamma_n\nu} \tag{8}$$

where ν_{n0} is the frequency, ν_{np} and γ_n are the spectral scaling and width of a resonance contributing to the permittivity function. The permittivity ε_∞ is a constant since the dielectric response at high frequencies is substantially detuned from the probe frequency. The real $\varepsilon_r(\nu)$ and imaginary $\varepsilon_i(\nu)$ parts of the permittivity function can be written separately as

$$\varepsilon_r(\nu) = \varepsilon_\infty + \sum_{n=1}^{N} \frac{\nu_{np}^2(\nu_{no}^2 - \nu^2)}{(\nu_{no}^2 - \nu^2)^2 + \gamma_n^2\nu^2} \quad \text{and} \quad \varepsilon_i(\nu) = \sum_{n=1}^{N} \frac{\nu_{np}^2\gamma_n\nu}{(\nu_{no}^2 - \nu^2)^2 + \gamma_n^2\nu^2} \ . \tag{9}$$

With respect to practical application, the absorption coefficient α and index of refraction n_r, given by

$$\alpha = \frac{4\pi\nu}{\sqrt{2}}\left[-\varepsilon_r + \sqrt{\varepsilon_r^2 + \varepsilon_i^2}\right]^{1/2} \quad \text{and} \quad n_r = \frac{1}{\sqrt{2}}\left[\varepsilon_r + \sqrt{\varepsilon_r^2 + \varepsilon_i^2}\right]^{1/2}, \tag{10}$$

respectively, provide direct relationships between calculated quantities obtained by DFT and "conveniently measurable" quantities α and n_r.

4

Case Study 1: Ground State Resonance Structure of β–HMX

In this section are presented two sets of data, which are the results of computational experiments using DFT, concerning the molecule β–HMX. These are the relaxed or equilibrium configuration of a single isolated molecule of β–HMX (see Table 1) and ground-state oscillation frequencies and IR intensities for this configuration that are calculated by DFT according to the frozen phonon approximation (see Table 2). A schematic representation of the molecular geometry of β–HMX is shown in Fig.(1).
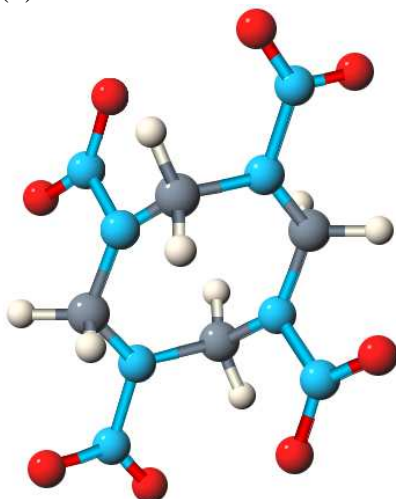

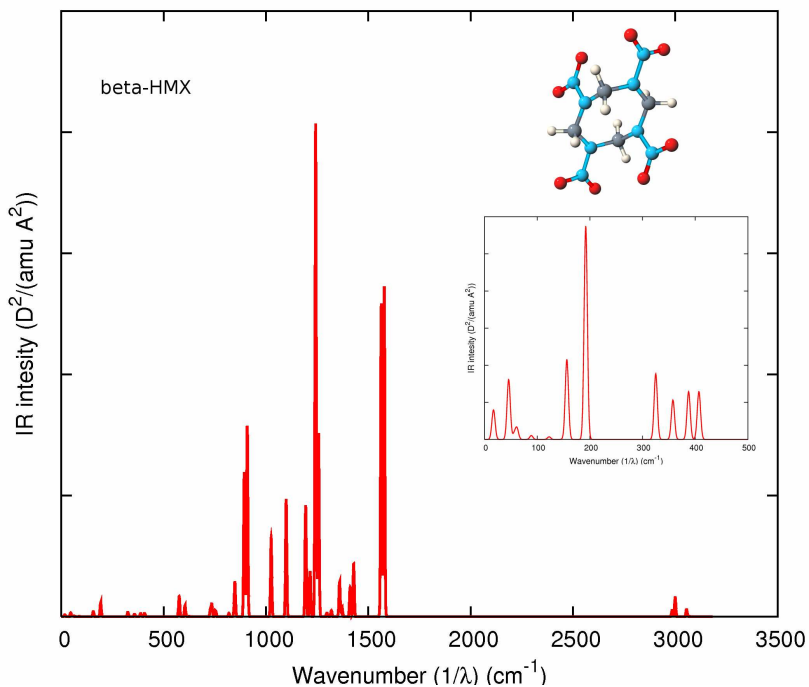**Figure 1.** Molecular Geometry of β–HMX.

Shown in Fig.(2) is the IR intensity as a function of frequency calculated using DFT for β–HMX according to a frozen phonon approximation. For the spectrum shown in Fig.(2), the structure of each resonance response is approximated essentially by that of a delta function.

Table 1. Atomic positions of β–HMX (Å)

Atomic number	X	Y	Z	Atomic number	X	Y	Z
6	-0.24112	2.38988	-0.2519	8	-0.51577	2.12311	-2.87632
6	-2.06734	0.627	-0.03867	8	-2.13048	0.63296	-2.67585
6	1.43622	0.44276	-0.06484	8	1.60928	3.89177	0.665
6	-0.39044	-1.31848	0.14565	8	3.1995	2.36492	0.62737
7	-1.12746	1.4121	-0.83025	8	-2.23149	-2.81763	-0.78797
7	1.13398	1.86281	-0.12373	8	-3.82907	-1.29822	-0.73707
7	0.49328	-0.33917	0.72518	1	-0.63362	2.67459	0.73503
7	-1.76538	-0.79316	0.01634	1	-0.2064	3.28046	-0.88724
7	0.62584	-0.31255	2.13416	1	-3.08482	0.69866	-0.44191
7	-1.27356	1.39698	-2.23846	1	-2.04603	1.05589	0.97174
7	2.05135	2.75994	0.44628	1	0.00366	-1.60125	-0.84102
7	-2.67908	-1.68961	-0.56012	1	-0.42275	-2.21059	0.77899
8	-0.14183	-1.03039	2.77	1	2.45279	0.37224	0.34102
8	1.48106	0.45171	2.57423	1	1.41841	0.01191	-1.07452

Table 2. Oscillation frequencies and IR intensities:

Frequency cm^{-1}	Intensity D^2/(amu Å^2)	Frequency cm^{-1}	Intensity D^2/(amu Å^2)	Frequency cm^{-1}	Intensity D^2/(amu Å^2)	Frequency cm^{-1}	Intensity D^2/(amu Å^2)
26.4866	0.0818	409.5643	0.0843	908.96	7.8913	1371.9015	0.3942
52.0196	0.1581	409.0395	0.0487	912.5801	0.0025	1388.269	0.0001
67.639	0.0136	574.8624	0.0003	1021.8896	0.0046	1411.1066	0.06
68.5724	0.0293	575.824	0.8315	1025.4058	3.2347	1411.1876	1.164
65.4672	0.0002	604.3452	0.4589	1098.9735	4.8331	1424.5004	0.0019
85.7122	123.1131	607.001	0.0003	1140.1849	0.0001	1429.6864	2.2004
88.7809	129.381	625.655	0.012	1179.3564	0.0008	1559.9806	0.0025
124.5233	0	628.2413	0.0001	1193.6798	4.572	1565.337	12.9842
135.4807	0.007	708.8374	0	1215.4229	1.9073	1577.0147	0.07
155.4847	0.0004	728.9038	0.3096	1219.0328	0.0093	1580.2385	13.6073
158.6671	0.2157	731.7556	0.0004	1233.6494	0.0007	2984.8881	0.0462
198.6825	0.5664	737.5166	0.4764	1241.195	20.3544	2985.496	0.2244
211.5764	0.0002	737.5396	0.0063	1257.4516	7.5375	2999.5538	0.7213
262.3964	0	755.5396	0.2272	1278.7335	0.0001	2998.4535	0.0822
283.9432	0	818.2214	0.0067	1288.5524	0.001	3053.2286	0.0779
327.8502	0.1775	819.2641	0.1317	1296.8519	0.1549	3053.9098	0.2106
330.3013	0.0001	847.9616	1.46	1313.5215	0.0001	3063.1195	0.0182
359.6587	0.1071	856.2495	0	1320.4272	0.2409	3063.1191	0.0105
388.2644	0.0013	894.1733	5.4895	1340.3144	0		
388.1113	0.1284	895.9141	0.5279	1359.9741	1.4318		

Figure 2. IR intensity as a function of frequency calculated using DFT for $\beta-$HMX according to frozen phonon approximation.
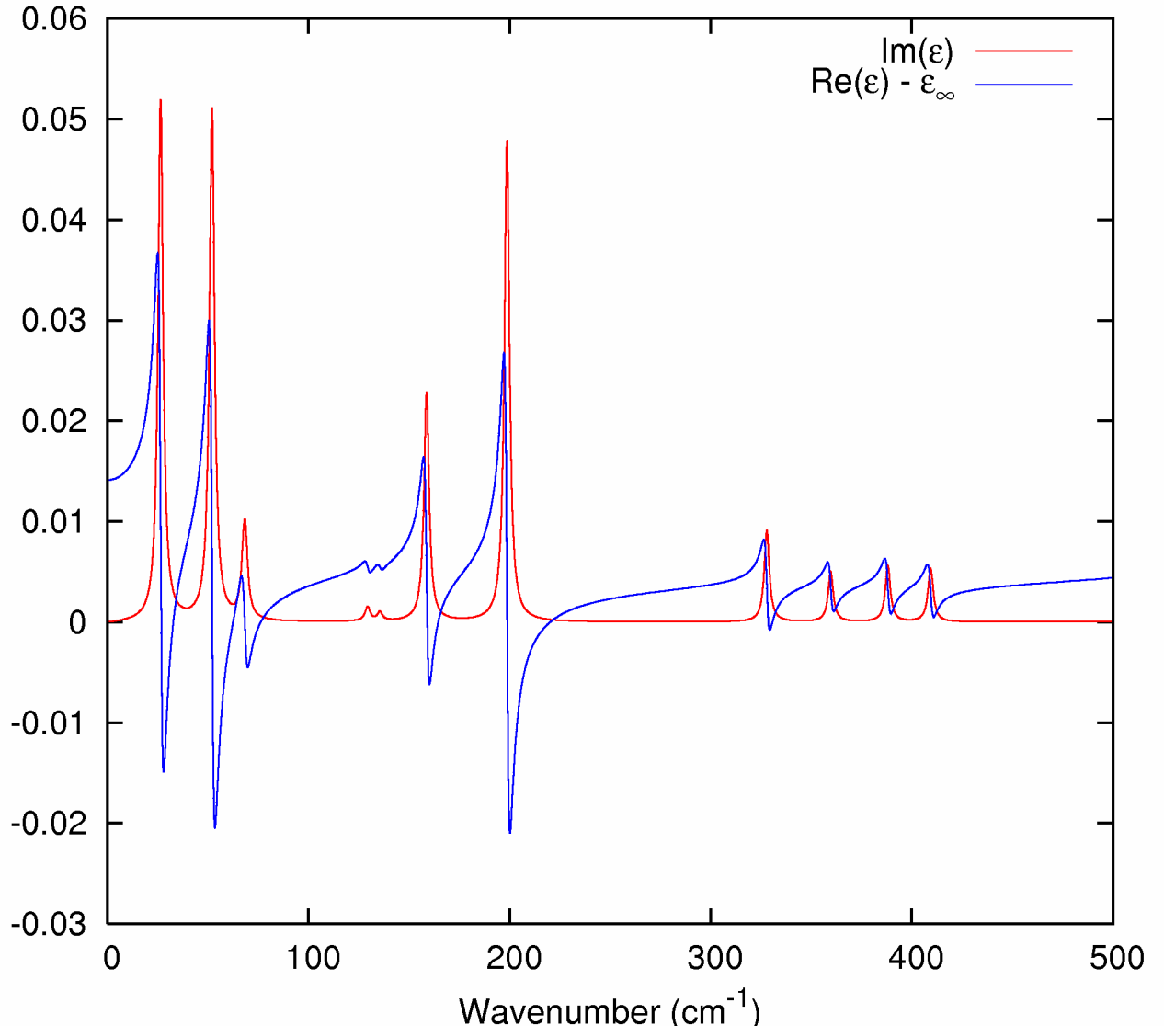
Figure 3. Real (blue) and imaginary (red) parts of permittivity function of $\beta-$HMX molecules with γ_n $= 3$ cm^{-1} and $\rho = 2.4 \cdot 10^{19}$ cm^{-3} for frequencies within THz range.

Case Study 2: Ground State Resonance Structure of PETN

In this section are presented two sets of data, which are the results of computational experiments using DFT, concerning the molecule PETN. These are the relaxed or equilibrium configuration of a single isolated molecule of PETN (see Table 3) and ground-state oscillation frequencies and IR intensities for this configuration that are calculated by DFT according to the frozen phonon approximation (see Table 4). A schematic representation of the molecular geometry of PETN is shown in Fig.(4).
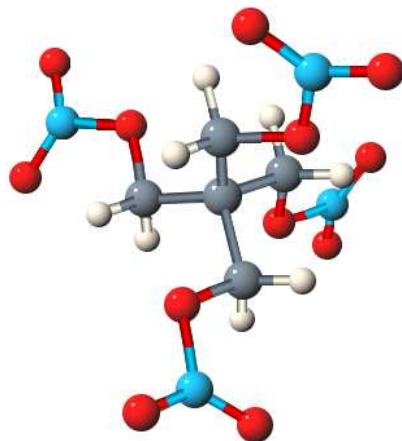

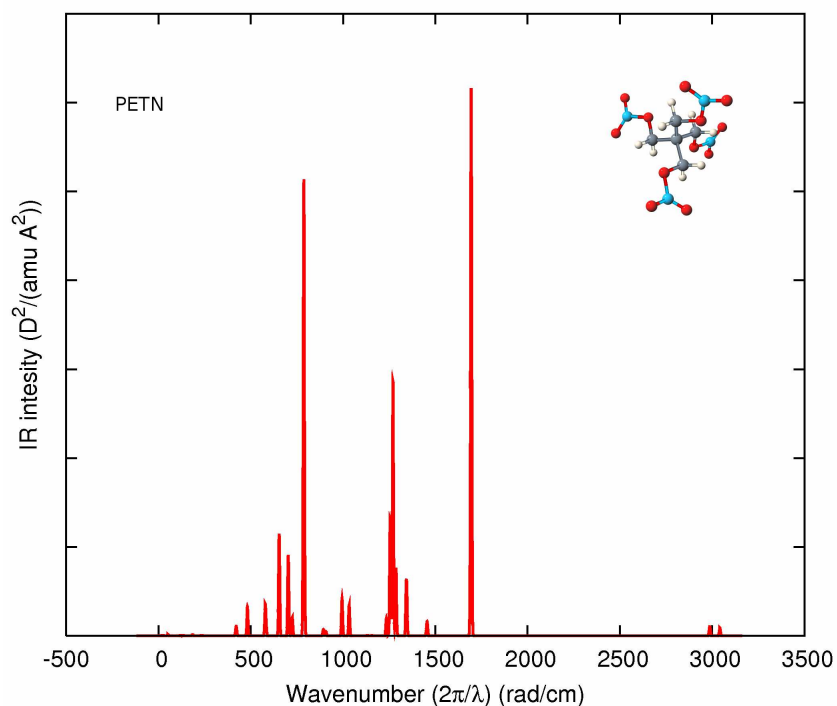**Figure 4.** Molecular Geometry of PETN.

Shown in Fig.(5) is the IR intensity as a function of frequency calculated using DFT for PETN according to a frozen phonon approximation. For the spectrum shown in Fig.(5), the structure of each resonance response is approximated essentially by that of a delta function.

Table 3. Atomic positions of PETN (Å).

Atomic number	X	Y	Z	Atomic number	X	Y	Z
6	-0.90787	0.48907	0.17354	8	1.94808	-3.14586	-0.03192
6	0.54956	0.01783	0.36869	8	2.80821	-1.21442	0.58616
6	-0.96651	2.01269	0.41718	1	-1.99624	2.37482	0.29107
6	-1.80732	-0.27726	1.16724	1	-0.31204	2.54022	-0.28938
6	-1.40666	0.20317	-1.25944	1	0.87858	0.19321	1.40132
8	-0.52463	2.24139	1.76964	1	1.21509	0.56308	-0.3142
8	0.58244	-1.39141	0.07067	1	-1.46281	-0.10281	2.19548
8	-3.14643	0.22812	0.99941	1	-1.78105	-1.35577	0.96103
8	-0.5109	0.88215	-2.1613	1	-2.43196	0.57423	-1.39229
8	-5.23155	0.00318	1.74575	1	-1.38953	-0.87791	-1.45237
8	-3.67634	-1.26381	2.65601	7	-4.11793	-0.42256	1.90605
8	-0.08736	3.85131	3.24351	7	-0.45302	3.67996	2.11044
8	-0.75847	4.4583	1.23535	7	1.93416	-1.97171	0.22886
8	-0.09204	1.22306	-4.32045	7	-0.85337	0.65487	-3.58248
8	-1.81642	-0.04519	-3.80006				

Table 4. Oscillation frequencies and IR intensities:

Frequency cm^{-1}	Intensity D^2/(amu Å^2)	Frequency cm^{-1}	Intensity D^2/(amu Å^2)	Frequency cm^{-1}	Intensity D^2/(amu Å^2)	Frequency cm^{-1}	Intensity D^2/(amu Å^2)
27.6924	0.0072	307.6541	0	893.5171	0.3109	1341.9832	0.9802
45.7692	0.0327	419.9976	0.2946	908.4957	0.1288	1345.3347	1.6302
75.5706	0.0023	420.3111	0.2982	907.8127	0.135	1358.2592	0.0004
65.4508	0.015	483.3724	1.6977	973.4102	0.0007	1450.6195	0.0268
82.2402	0.0111	555.0496	0.0005	995.1452	1.022	1451.8016	0.0914
85.8255	0.0045	577.1765	0.8504	995.8256	1.0268	1456.0802	0.397
52.9438	0.0048	579.001	0.8601	1024.0042	0.0008	1456.6128	0.3994
78.9206	0.0323	583.1426	0.2211	1033.1369	1.8175	1690.1603	1.0193
77.8851	0.0334	609.0535	0.0006	1133.8946	0.0215	1692.9065	7.8371
124.1609	0.0096	652.6221	2.8048	1157.0829	0.0091	1693.0525	12.4003
124.381	0.0072	651.6133	2.7891	1157.2312	0.0092	1697.4129	11.0743
145.0029	0.0471	704.123	4.6868	1216.6553	0.0005	2982.9778	0.1752
146.806	0.0001	727.4008	0.1249	1234.5454	0.494	2985.3071	0.2
171.1139	0.0014	726.4067	0.1068	1235.3559	0.514	2984.8943	0.1837
192.1037	0.0366	727.571	0.1801	1254.1184	6.7697	2986.1399	0.0196
192.0644	0.0295	728.1667	0.8163	1267.8336	6.9384	3035.5243	0.0363
196.0122	0.0006	787.2791	7.1124	1267.4456	6.9192	3038.1006	0.0998
237.8431	0.0229	787.7443	7.1507	1280.9494	0.0544	3038.8521	0.1325
240.7368	0.014	788.9399	12.423	3039.7682	0.2253		
242.4609	0.0059	802.3902	0.0015	1284.8749	4.0339		
295.694	0.0012	825.5549	0.0012	1342.235	1		

Figure 5. IR intensity as a function of frequency calculated using DFT for PETN according to frozen phonon approximation.
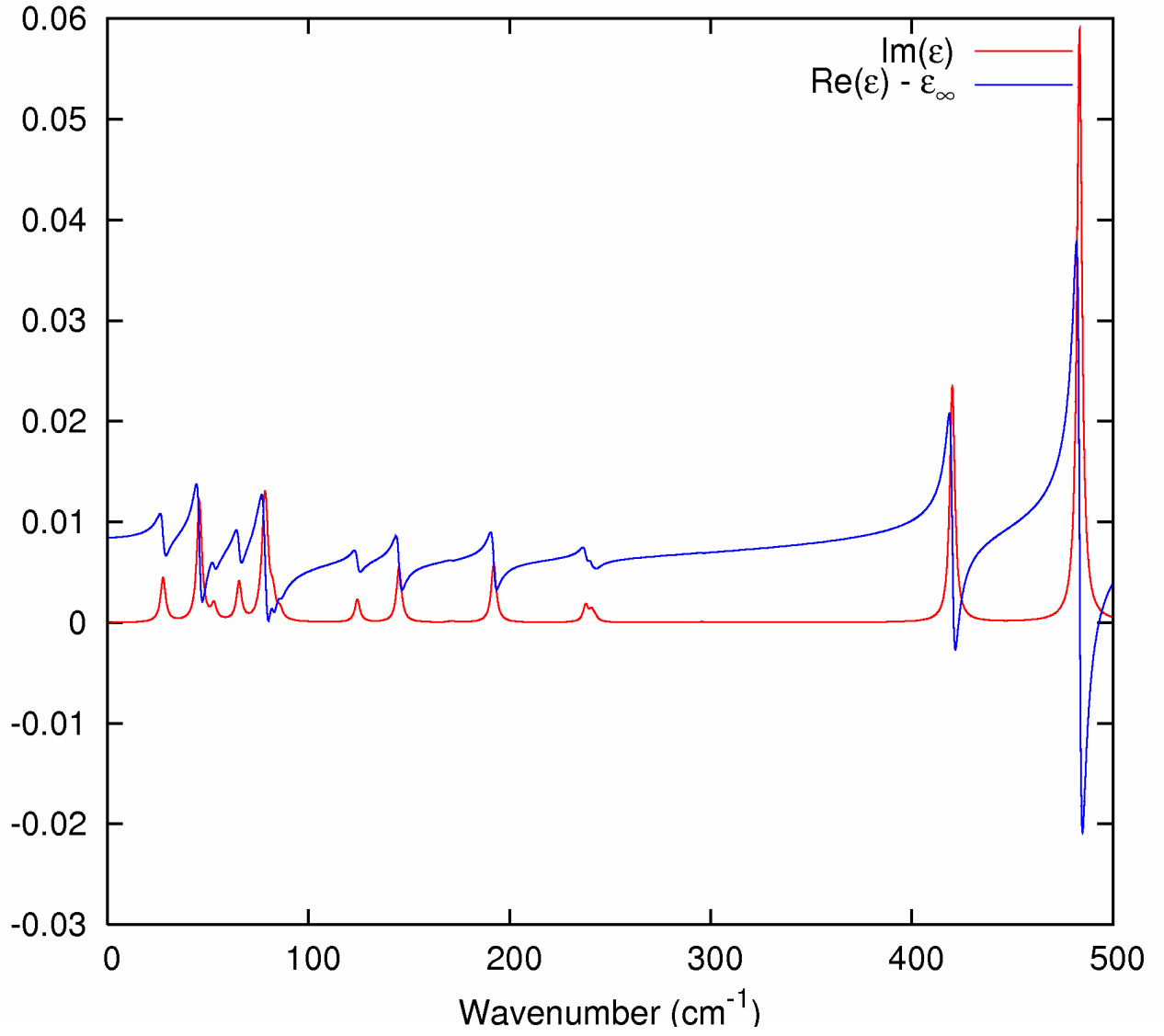
Figure 6. Real (blue) and imaginary (red) parts of permittivity function of PETN molecules with $\gamma_n = 3$ cm^{-1} and $\rho = 2.4 \cdot 10^{19}$ cm^{-3} for frequencies within THz range.

Case Study 3: Ground State Resonance Structure of RDX

In this section are presented two sets of data, which are the results of computational experiments using DFT, concerning the molecule RDX. These are the relaxed or equilibrium configuration of a single isolated molecule of RDX (see Table 5) and ground-state oscillation frequencies and IR intensities for this configuration that are calculated by DFT according to the frozen phonon approximation (see Table 6). A schematic representation of the molecular geometry of RDX is shown in Fig.(7).
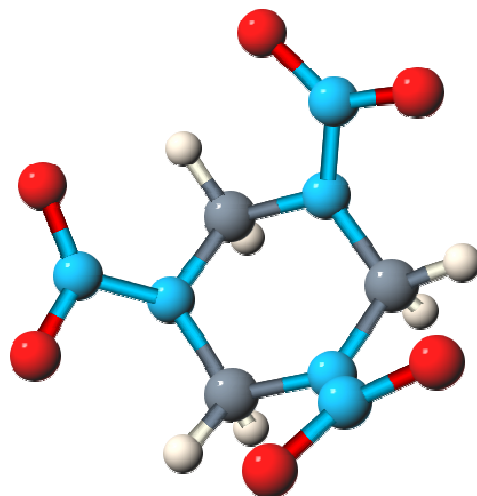

Figure 7. Molecular Geometry of RDX.

Shown in Fig.(8) is the IR intensity as a function of frequency calculated using DFT for RDX according to a frozen phonon approximation. For the spectrum shown in Fig.(8), the structure of each resonance response is approximated essentially by that of a delta function.

Table 5. Atomic positions of RDX (Å):

Atomic number	X	Y	Z	Atomic number	X	Y	Z
7	1.16994	-0.81313	0.09076	8	-1.12995	1.87973	2.52487
7	0.09076	1.16994	-0.81313	8	3.34946	-0.19764	0.06923
7	-0.81313	0.09076	1.16994	8	0.06923	3.34946	-0.19764
7	2.44674	-0.67765	0.7438	8	-0.19764	0.06923	3.34946
7	0.7438	2.44674	-0.67765	1	-1.50333	1.88316	0.33719
7	-0.67765	0.7438	2.44674	1	0.33719	-1.50333	1.88316
6	-1.09011	0.92662	0.00735	1	1.88316	0.33719	-1.50333
6	0.00735	-1.09011	0.92662	1	-1.82611	0.39667	-0.61584
6	0.92662	0.00735	-1.09011	1	-0.61584	-1.82611	0.39667
8	2.52487	-1.12995	1.87973	1	0.39667	-0.61584	-1.82611
8	1.87973	2.52487	-1.12995				

Table 6. Oscillation frequencies and IR intensities:

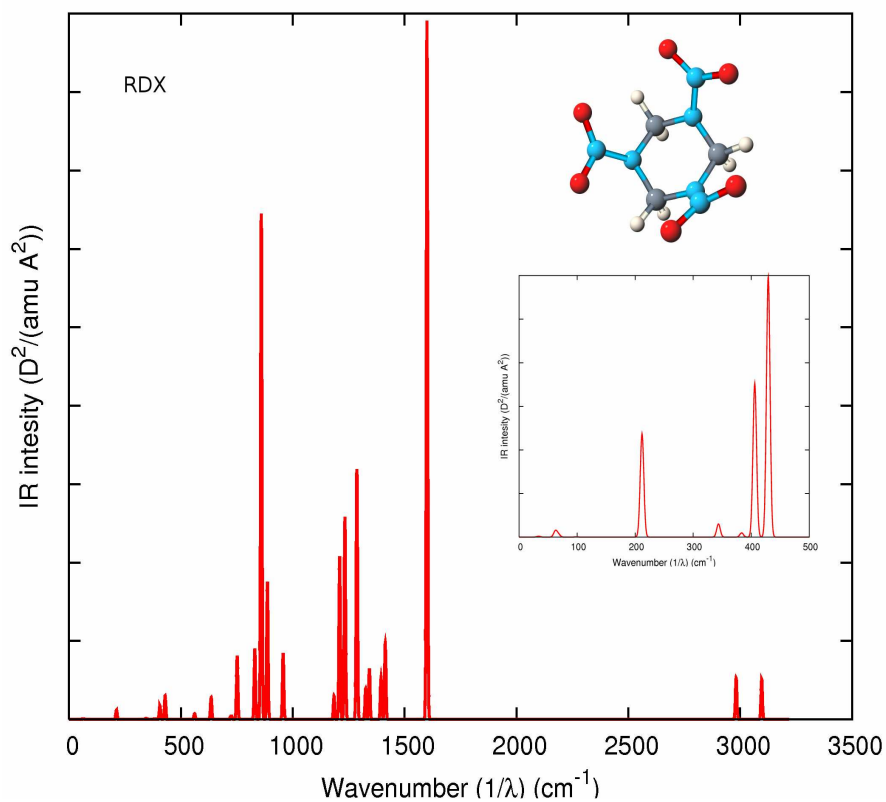| Frequency cm^{-1}	Intensity D^2/(amu Å^2)	Frequency cm^{-1}	Intensity D^2/(amu Å^2)	Frequency cm^{-1}	Intensity D^2/(amu Å^2)	Frequency cm^{-1}	Intensity D^2/(amu Å^2)
50.4476	0.0012	561.592	0.068	958.8454	0.841	1394.1574	0.5447
51.1589	0.0012	561.6381	0.0682	958.8824	0.8369	1395.0201	0.5394
77.7345	0.0128	573.1913	0.0001	1106.4304	0	1414.4218	1.9899
91.1576	0.0081	635.6372	0.2794	1185.1197	0.598	1572.3865	0.0002
125.232	0.0004	635.8515	0.2799	1208.9255	2.0878	1600.7625	8.9248
125.1679	0.0004	723.8626	0.0454	1209.0906	2.0855	1600.6959	8.9225
215.3785	0.1185	728.3136	0.0363	1218.0051	0.0005	2979.9541	0.0238
215.3755	0.1184	728.3277	0.036	1231.9493	2.5768	2980.1722	0.0204
290.8681	0.0001	752.231	1.6486	1231.8716	2.5783	2983.6473	1.0283
346.3176	0.0151	830.6969	0.908	1284.8248	6.3921	3098.3191	0.3366
346.2359	0.0151	830.9032	0.9079	1304.8515	0.0003	3099.4052	0.3341
392.0173	0.0047	859.1975	6.4437	1326.7768	0.368	3096.9028	0.4219
391.356	0.0047	858.8267	6.4375	1327.4575	0.3693		
413.5828	0.3457	863.9551	0.0141	1344.0359	0.6348		
431.3056	0.5958	886.788	3.5023	1344.7081	0.6313		

Figure 8. IR intensity as a function of frequency calculated using DFT for RDX according to frozen phonon approximation.
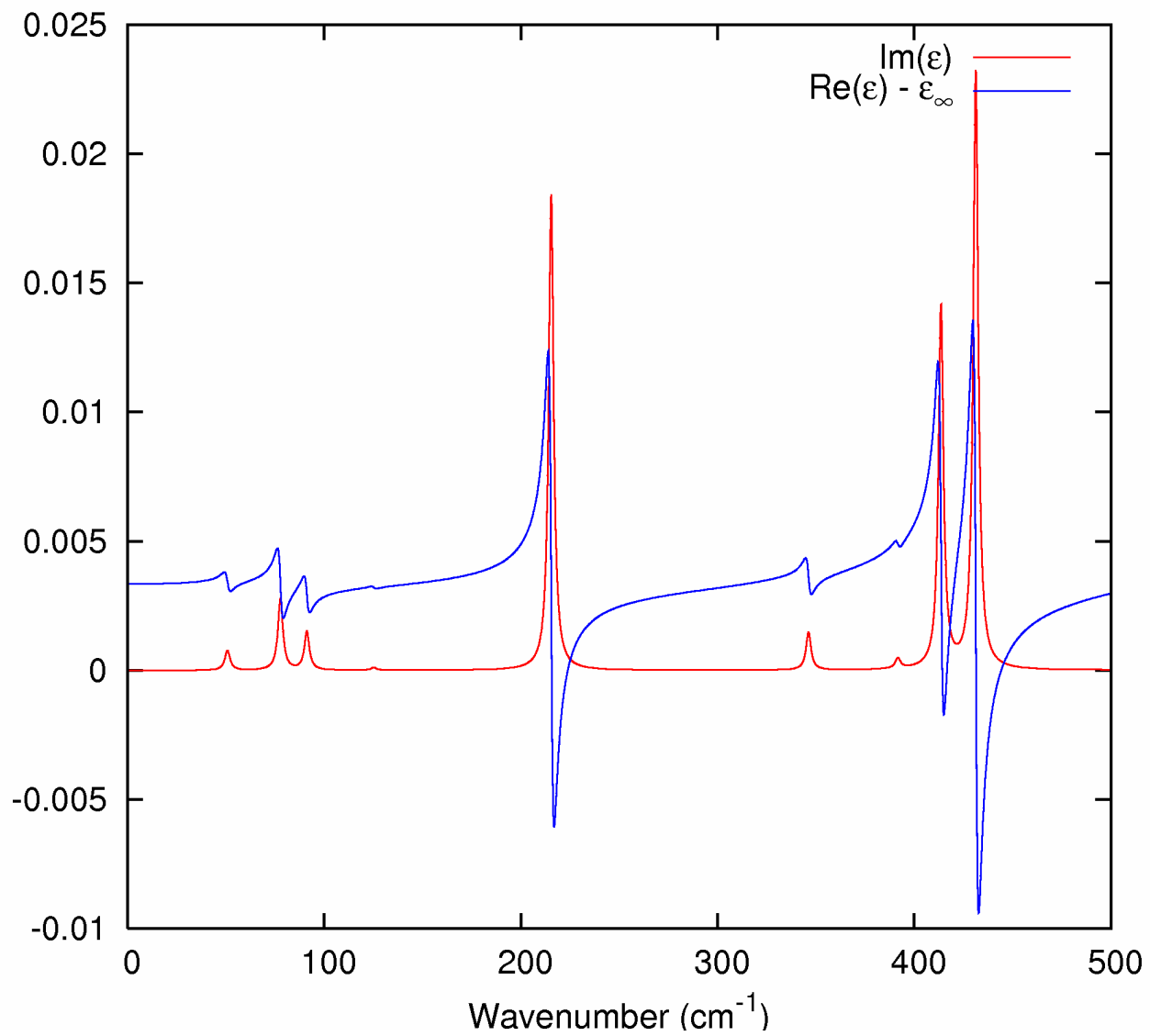
Figure 9. Real (blue) and imaginary (red) parts of permittivity function of RDX molecules with $\gamma_n = 3$ cm^{-1} and $\rho = 2.4 \cdot 10^{19}$ cm^{-3} for frequencies within THz range.

Case Study 4: Ground State Resonance Structure of TNT1

In this section are presented two sets of data, which are the results of computational experiments using DFT, concerning the molecule TNT1. These are the relaxed or equilibrium configuration of a single isolated molecule of TNT1 (see Table 7) and ground-state oscillation frequencies and IR intensities for this configuration that are calculated by DFT according to the frozen phonon approximation (see Table 8). A schematic representation of the molecular geometry of TNT1 is shown in Fig.(10).
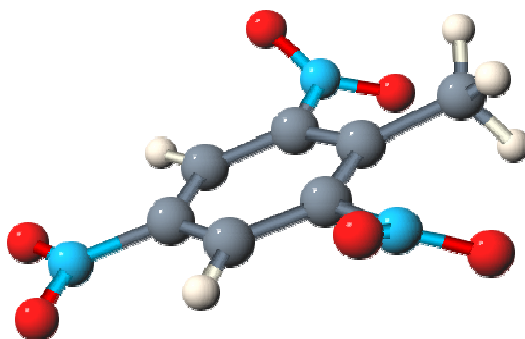

Figure 10. Molecular Geometry of TNT1.

Shown in Fig.(11) is the IR intensity as a function of frequency calculated using DFT for TNT1 according to a frozen phonon approximation. For the spectrum shown in Fig.(11), the structure of each resonance response is approximated essentially by that of a delta function.

Table 7. Atomic positions of TNT1 (Å):

Atomic number	X	Y	Z	Atomic number	X	Y	Z
1	1.277	-0.71765	1.9543	6	1.41827	-0.47815	-2.75813
1	-2.49724	-0.7602	-0.12405	7	-1.38812	-0.82281	2.33281
1	0.77359	-0.73572	-3.60038	7	2.83728	-0.47406	-0.14338
1	2.29092	-1.14373	-2.77796	7	-1.56142	-0.74062	-2.57029
1	1.80338	0.54246	-2.88489	8	3.37643	0.34145	-0.89378
6	0.71266	-0.68704	1.02471	8	3.41117	-1.19787	0.67094
6	-0.67498	-0.7428	1.03277	8	-0.69699	-0.7987	3.35263
6	-1.40976	-0.72761	-0.14562	8	-2.61686	-0.90672	2.29484
6	-0.71255	-0.68459	-1.3493	8	-2.49644	0.05804	-2.62488
6	0.69021	-0.58801	-1.44921	8	-1.28456	-1.59556	-3.41343
6	1.35505	-0.58239	-0.20393				

Table 8. Oscillation frequencies and IR intensities:

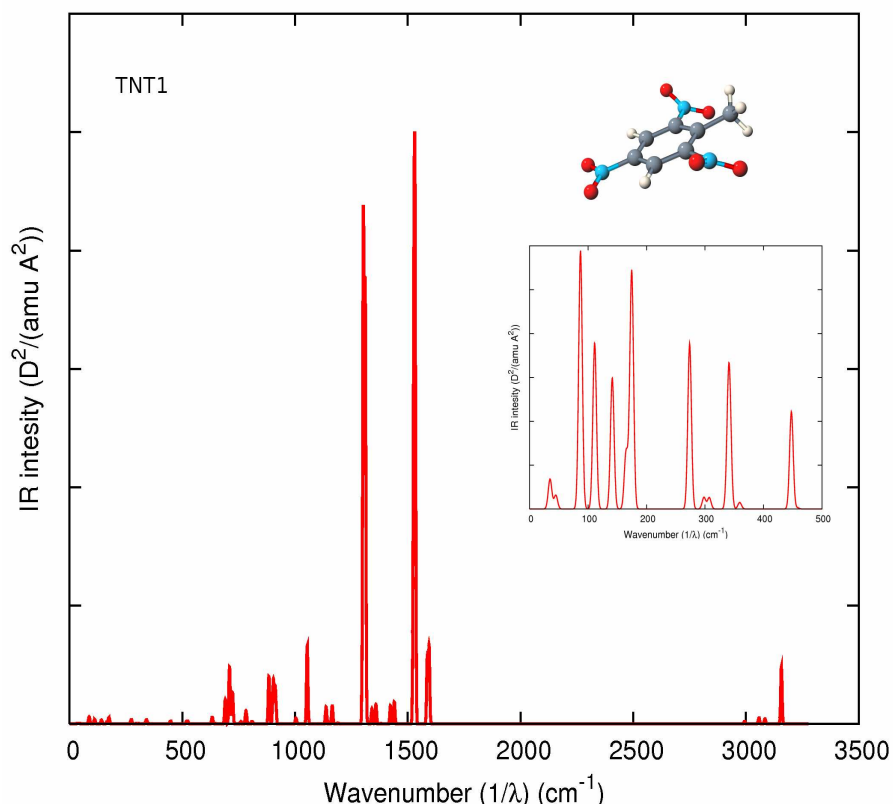| Frequency cm^{-1}	Intensity D^2/(amu Å^2)	Frequency cm^{-1}	Intensity D^2/(amu Å^2)	Frequency cm^{-1}	Intensity D^2/(amu Å^2)	Frequency cm^{-1}	Intensity D^2/(amu Å^2)
172.5174	0.0237	414.8762	0.0385	908.0919	0.4081	1449.4697	0.2159
197.4056	0.011	495.2412	0.0797	913.9983	0.5736	1487.7755	0.4935
135.2506	0.001	522.6106	0.0393	1057.9824	0.0914	1528.3766	4.1144
284.1745	0.0427	560.2942	0.0077	1068.9096	0.1036	1524.3186	6.5037
361.7698	0.012	578.169	0.0073	1057.3348	1.2247	1532.7054	3.8635
427.1822	0.133	668.3243	0.432	1137.2714	0.3466	1585.1704	1.0497
172.7674	0.0458	702.98	0.0633	1177.5714	0.2562	1592.6665	0.7857
171.747	0.0908	709.4691	1.031	1190.6768	0.0231	2804.9617	0.0052
177.736	0.0114	733.5913	0.398	1301.8607	8.6558	2860.6966	0.0794
285.6632	0.0627	744.7193	0.1154	1308.2775	7.0606	2930.3248	0.053
300.4711	0.0241	768.8811	0.017	1325.0594	0.5661	3154.161	0.4024
304.604	0.0077	783.0319	0.2198	1355.3609	0.1079	3160.6014	0.5166
337.6068	0.0188	808.5178	0.0437	1385.5683	0.2682		
342.8559	0.0512	889.7004	0.8604	1386.0299	0.0801		
376.9598	0.053	907.8869	0.4586	1462.453	0.0542		

Figure 11. IR intensity as a function of frequency calculated using DFT for TNT1 according to frozen phonon approximation.
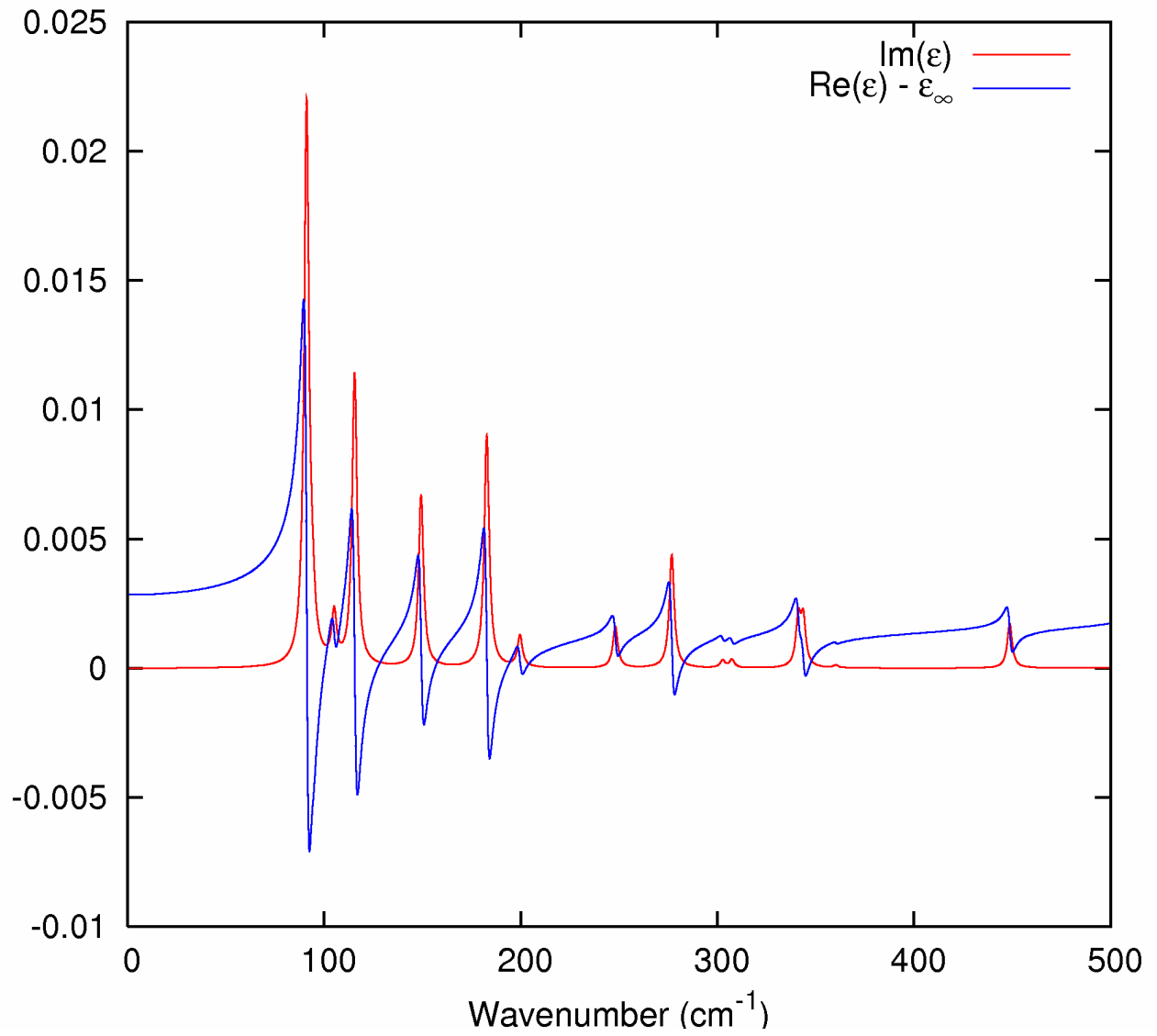
Figure 12. Real (blue) and imaginary (red) parts of permittivity function of TNT1 molecules with $\gamma_n = 3$ cm^{-1} and $\rho = 2.4 \cdot 10^{19}$ cm^{-3} for frequencies within THz range.

Case Study 5: Ground State Resonance Structure of TNT2

In this section are presented two sets of data, which are the results of computational experiments using DFT, concerning the molecule TNT2. These are the relaxed or equilibrium configuration of a single isolated molecule of TNT2 (see Table 9) and ground-state oscillation frequencies and IR intensities for this configuration that are calculated by DFT according to the frozen phonon approximation (see Table 10). A schematic representation of the molecular geometry of TNT2 is shown in Fig.(13).
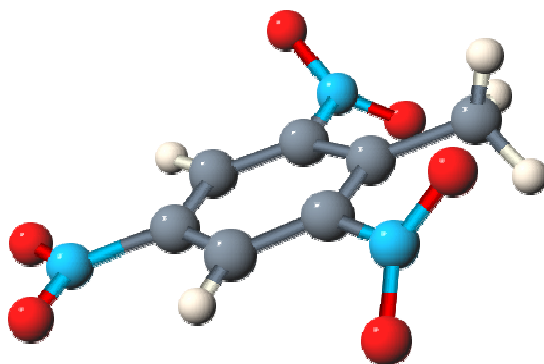

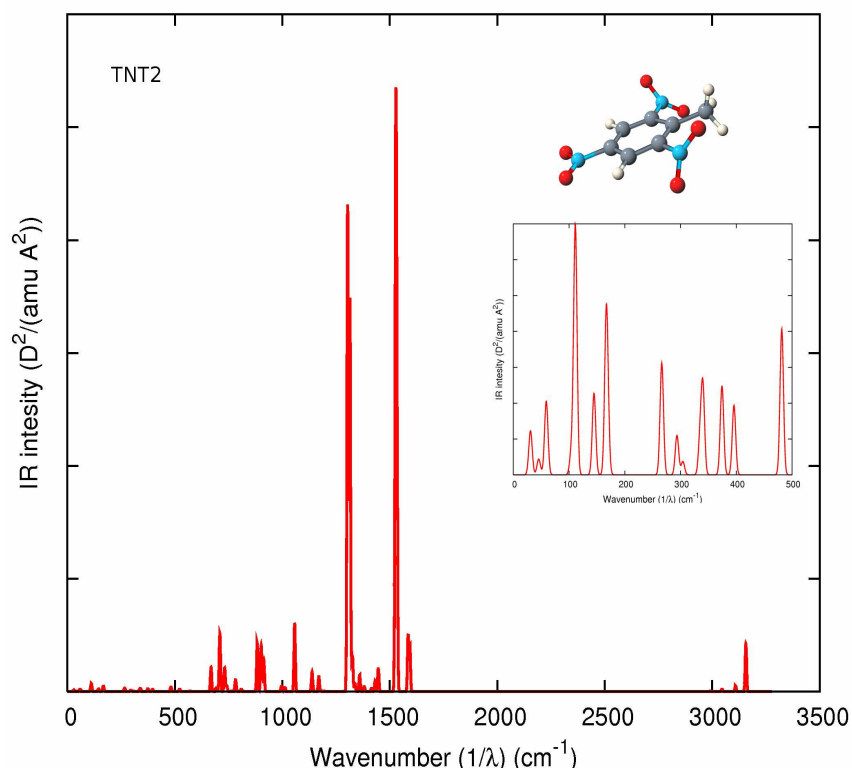**Figure 13.** Molecular Geometry of TNT2.

Shown in Fig.(14) is the IR intensity as a function of frequency calculated using DFT for TNT2 according to a frozen phonon approximation. For the spectrum shown in Fig.(14), the structure of each resonance response is approximated essentially by that of a delta function.

Table 9. Atomic positions of TNT2 (Å):

Atomic number	X	Y	Z	Atomic number	X	Y	Z
1	1.277	-0.71765	1.9543	6	1.41827	-0.47815	-2.75813
1	-2.49724	-0.7602	-0.12405	7	-1.38812	-0.82281	2.33281
1	0.77359	-0.73572	-3.60038	7	2.83728	-0.47406	-0.14338
1	2.29092	-1.14373	-2.77796	7	-1.56142	-0.74062	-2.57029
1	1.80338	0.54246	-2.88489	8	3.37643	0.34145	-0.89378
6	0.71266	-0.68704	1.02471	8	3.41117	-1.19787	0.67094
6	-0.67498	-0.7428	1.03277	8	-0.69699	-0.7987	3.35263
6	-1.40976	-0.72761	-0.14562	8	-2.61686	-0.90672	2.29484
6	-0.71255	-0.68459	-1.3493	8	-2.49644	0.05804	-2.62488
6	0.69021	-0.58801	-1.44921	8	-1.28456	-1.59556	-3.41343
6	1.35505	-0.58239	-0.20393				

Table 10. Oscillation frequencies and IR intensities:

Frequency cm^{-1}	Intensity D^2/(amu Å^2)	Frequency cm^{-1}	Intensity D^2/(amu Å^2)	Frequency cm^{-1}	Intensity D^2/(amu Å^2)	Frequency cm^{-1}	Intensity D^2/(amu Å^2)
172.5174	0.0237	414.8762	0.0385	908.0919	0.4081	1449.4697	0.2159
197.4056	0.011	495.2412	0.0797	913.9983	0.5736	1487.7755	0.4935
135.2506	0.001	522.6106	0.0393	1057.9824	0.0914	1528.3766	4.1144
284.1745	0.0427	560.2942	0.0077	1068.9096	0.1036	1524.3186	6.5037
361.7698	0.012	578.169	0.0073	1057.3348	1.2247	1532.7054	3.8635
427.1822	0.133	668.3243	0.432	1137.2714	0.3466	1585.1704	1.0497
172.7674	0.0458	702.98	0.0633	1177.5714	0.2562	1592.6665	0.7857
171.747	0.0908	709.4691	1.031	1190.6768	0.0231	2804.9617	0.0052
177.736	0.0114	733.5913	0.398	1301.8607	8.6558	2860.6966	0.0794
285.6632	0.0627	744.7193	0.1154	1308.2775	7.0606	2930.3248	0.053
300.4711	0.0241	768.8811	0.017	1325.0594	0.5661	3154.161	0.4024
304.604	0.0077	783.0319	0.2198	1355.3609	0.1079	3160.6014	0.5166
337.6068	0.0188	808.5178	0.0437	1385.5683	0.2682		
342.8559	0.0512	889.7004	0.8604	1386.0299	0.0801		
376.9598	0.053	907.8869	0.4586	1462.453	0.0542		

Figure 14. IR intensity as a function of frequency calculated using DFT for TNT2 according to frozen phonon approximation.
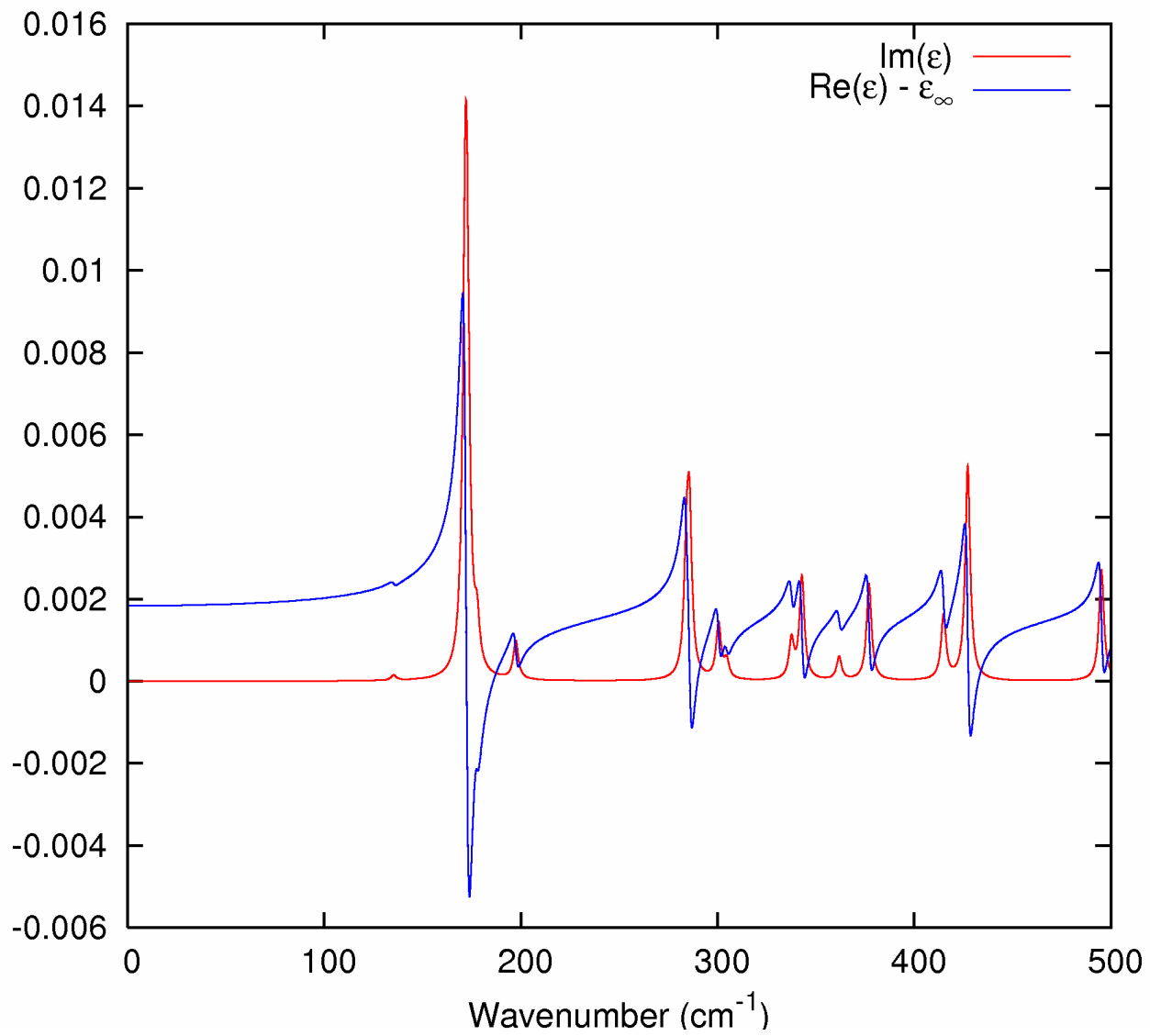
Figure 15. Real (blue) and imaginary (red) parts of permittivity function of TNT2 molecules with $\gamma_n = 3$ cm^{-1} and $\rho = 2.4 \cdot 10^{19}$ cm^{-3} for frequencies within THz range.

Discussion

The DFT calculated absorption spectra given in tables 2, 4, 6 and 8 provide two types of information for general analysis of dielectric response. These are the denumeration of ground state resonance modes and estimates of molecular level dielectric response structure. The construction of permittivity functions using the DFT calculated absorption spectra follows the same procedure as that applied for the construction of permittivity functions using experimentally measured absorption spectra, but with the addition of certain constraint conditions. Accordingly, construction of permittivity functions using either DFT or experimentally measured absorption spectra requires parameterizations that are in terms of physically consistent analytic function representations such as the Drude-Lorentz model. Although the formal structure of permittivity functions constructed using DFT and experimental measurements are the same, their interpretation with respect to parameterization is different for each case.

The construction of permittivity functions using experimental measurements, an established methodology, defines an inverse problem where resonant locations, peaks and widths, as well as the number of resonances, are assumed adjustable. Following this approach, it follows that many of the detailed characteristics of resonance structure are smoothed or averaged. In addition, measurement artifacts associated with sample preparation and detector configuration can in principle introduce errors. One advantage of permittivity functions constructed using experimental measurements, however, is that many aspects of dielectric response on the macroscale that are associated with multiscale averaging and molecule-lattice coupling are taken into account inherently. Accordingly, the disadvantage of this approach is that the nature of any multiscale averaging and resonant structure, contributing to dielectric response on the macroscopic level, may not be understood. This lack of quantitative understanding can in principle inhibit the development of pump-probe type methodologies for selective excitation of molecular modes, which are for the purpose of enhanced signature detection or modulation.

The construction of permittivity functions using DFT calculations, the methodology whose development is considered here, defines a direct problem approach where dielectric response is estimated within the bounds of relatively well-defined adjustable parameters. Following this approach, a permittivity function is constructed using the DFT calculated absorption spectra, e.g., tables 2, 4, 6, 8 and 10, under the condition that the calculated resonance locations are fixed, while resonance widths and number densities are assumed adjustable, e.g., Figs. (3), (6), (9), (12) and (15). Better interpretation of dielectric response of explosives on a macroscale can be achieved through correlation of resonance structure that is experimentally observed and calculated by DFT. In principle, correlation of resonance structure would include the quantitative analysis of changes in signature features associated with the transition of the system from that of a low-density system of uncoupled molecule to that of a bulk lattice.

With respect to more extensive DFT calculations concerning the ground-state absorption spectra of a bulk lattice or spectra corresponding to electronic state transitions, it is important to note that the atomic positions of the relaxed or equilibrium configuration of a single isolated molecule, e.g., tables 1, 3, 5, 7 and 9, provide a convenient starting point. Calculation of the dielectric response of a bulk lattice would entail, in principle, the construction of a super cell consisting of molecules whose initial positions are those determined by DFT for isolated systems. Additional constraints on this super cell could be based on crystallographic information concerning bulk density or lattice spacing. Calculation of the dielectric response associated with electronic state transitions would entail the application of methods based on perturbation theory. In principle, for these methods most of the computational effort is expended for determination of the ground state, with respect to which all excited states are determined self consistently. These methods typically would be based on time-dependent density functional theory (TDDFT).

Conclusion

The calculations of ground state resonance structure associated with the high explosives β–HMX, PETN, RDX, TNT1 and TNT2 using DFT are meant to serve as reasonable estimates of molecular level response characteristics, providing interpretation of dielectric response features, for subsequent adjustment relative to experimental measurements and molecular structure theory.

Acknowledgement

Appendix 1

General Framework for Numerical Simulation of IED Detection and Remote Activation Scenarios

The set of parameterized permittivity functions given above represent contributions to a component model of a general framework for numerical simulation of IED detection and remote activation scenarios, whose initial construction was described in reference 14 (see Fig.(A1)). In addition, the discussions concerning NRLMOL given above, as well as previously [14], provide information concerning the practical application of NRLMOL for construction of dielectric response functions. Accordingly, included in this appendix are notes describing modifications and errata associated with the continuous evolution of this framework for purposes of practical analysis and simulation. In particular, included in this appendix are corrections to the S-matrix computer program presented in reference 14.
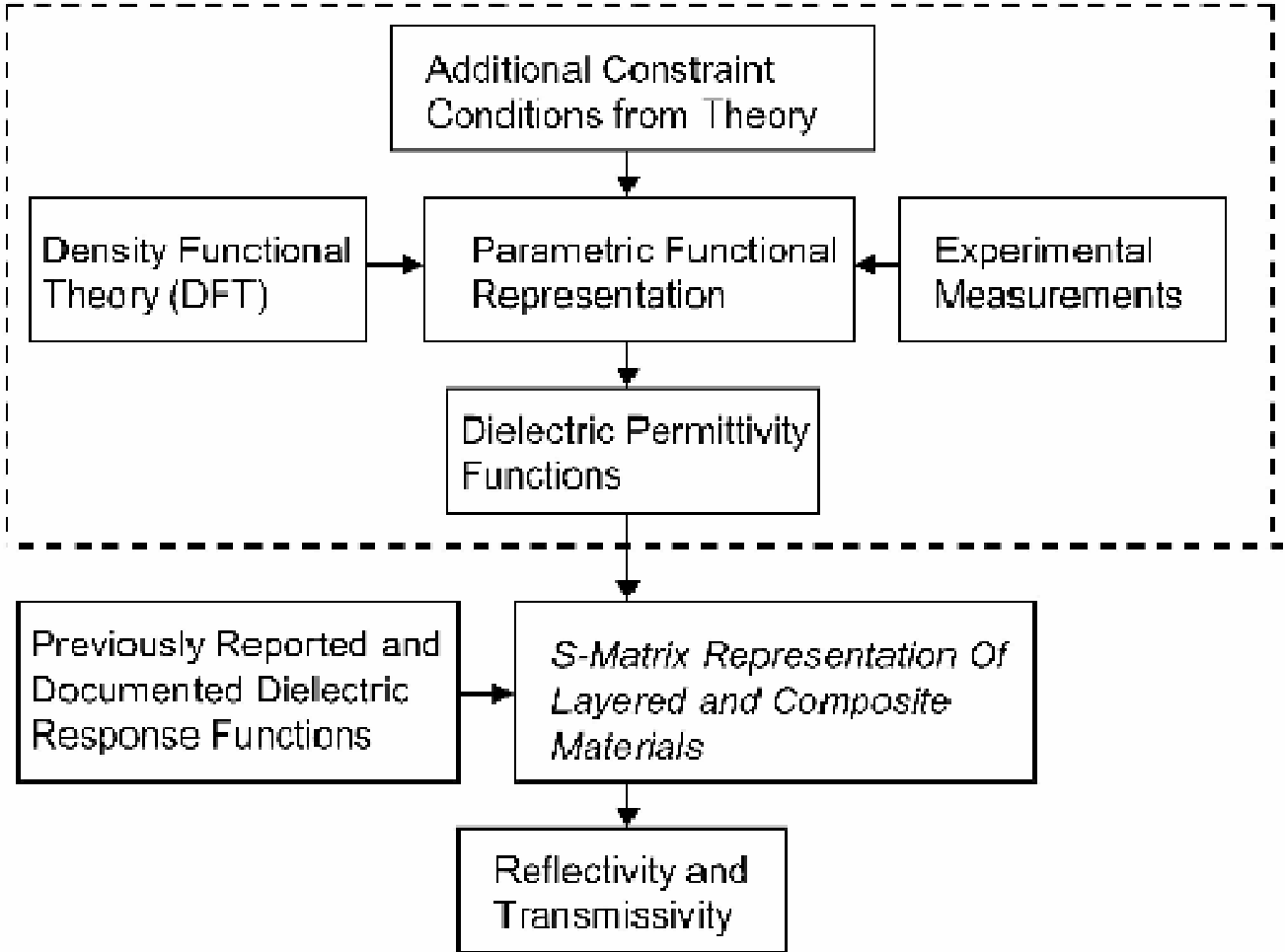

Figure A1. General framework for numerical simulation of IED detection.

Discussion Concerning General Framework for Numerical Simulation of IED detection.

The general framework for numerical simulation of IED detection and remote activation scenarios presented in reference 14 places emphasis on the construction of permittivity functions using DFT calculated spectra, their parameterization and parameter adjustment with respect to additional information, which are for input to an S-matrix representation of a layered and composite system. It is significant to note, however, that from a practical perspective, the construction of permittivity functions using DFT represents one of three approaches to inputting information concerning dielectric response of materials to a general framework based on an S-matrix representation. These other approaches are: construction of permittivity functions by inverse analysis of experimentally measured spectra; and the use of permittivity functions that have been previously reported and documented. Accordingly, a schematic of the general framework for numerical simulation of IED detection is shown in Fig.(A1), which describes the interrelation between three approaches for inputting information concerning dielectric response of materials to the S-matrix representation. Referring to Fig.(A1), it is to be noted that construction of permittivity functions using DFT calculated spectra and experimentally measured spectra follow approaches that are similar, and therefore represent a single component of the general framework, which is shown as contained within dashed lines. Referring again to Fig.(A1), it is seen that from the perspective of practical analysis, a data base consisting of previously reported and documented permittivity functions represents a component of the general framework that extends its capability with respect to simulation of complex systems. In particular, the response signatures of permittivity functions constructed using DFT calculated spectra and experimentally measured spectra can be examined as they occur in combination with materials whose dielectric response has already been well documented quantitatively, e.g., metals [15] and water [16,17].

Itemized corrections of figures presented in reference 14.

In Fig.(3) of reference 14, the x-axis scale should be multiplied by 2π for correct values of the wavenumber. In addition, this figure does not shows the resonances bellow 300 cm^{-1}($\approx 50\times 2\pi$ cm^{-1}). For frequencies lower than 300 cm^{-1}, the permittivity function of β-HMX is shown in Fig.(A2).
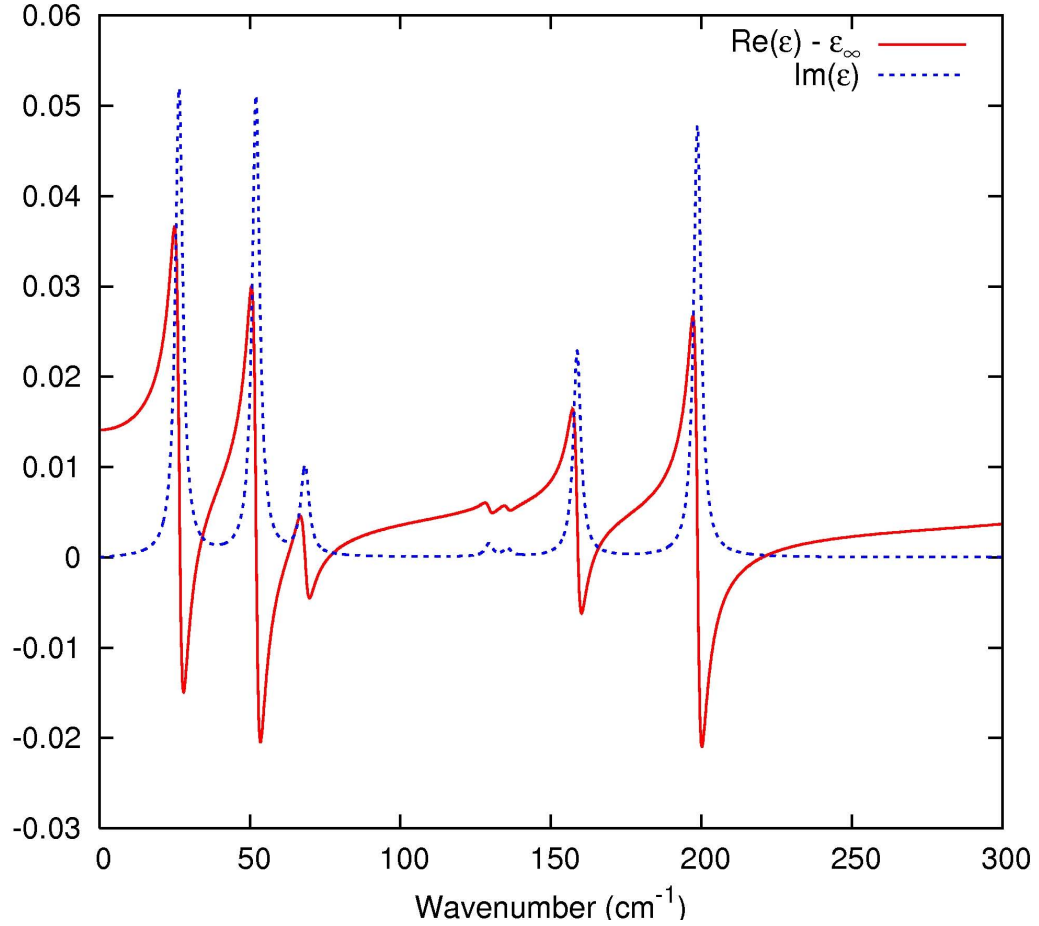
Figure A2. Permittivity function of β-HMX for frequencies within THz range.

In Fig.(4) of reference 14, the x-axis scale should be multiplied by 2π for correct values of the wavenumber. For frequencies lower than 300 cm^{-1}($\approx 50 \times 2\pi$ cm^{-1}), the reflectivity function R_s is shown in Fig.(A3) for an optically dense layer of β–HMX molecules with $\varepsilon_\infty = 1$ (upper) and $\varepsilon_\infty = 1.2$ (lower).
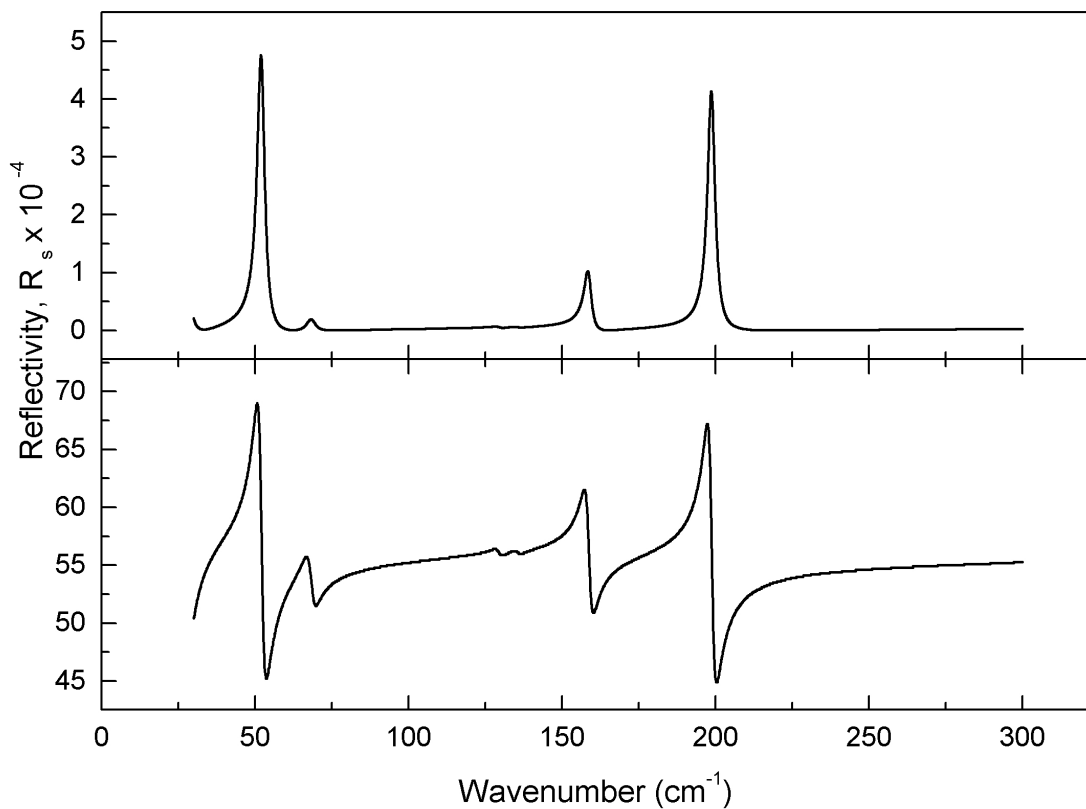

Figure A3. Reflectivity functions for a layer of β–HMX on a gold substrate.

In Figs. (7) and (8) of reference 14, the x-axis scale should be multiplied by 2π for correct values of the wavenumber. For frequencies lower than 300 cm^{-1}($\approx 50 \times 2\pi$ cm^{-1}), the absorption coefficient and index of refraction are shown in the Fig.(A4) for $\gamma = 3$ cm^{-1} and $N = 4$ cm^{-2}.
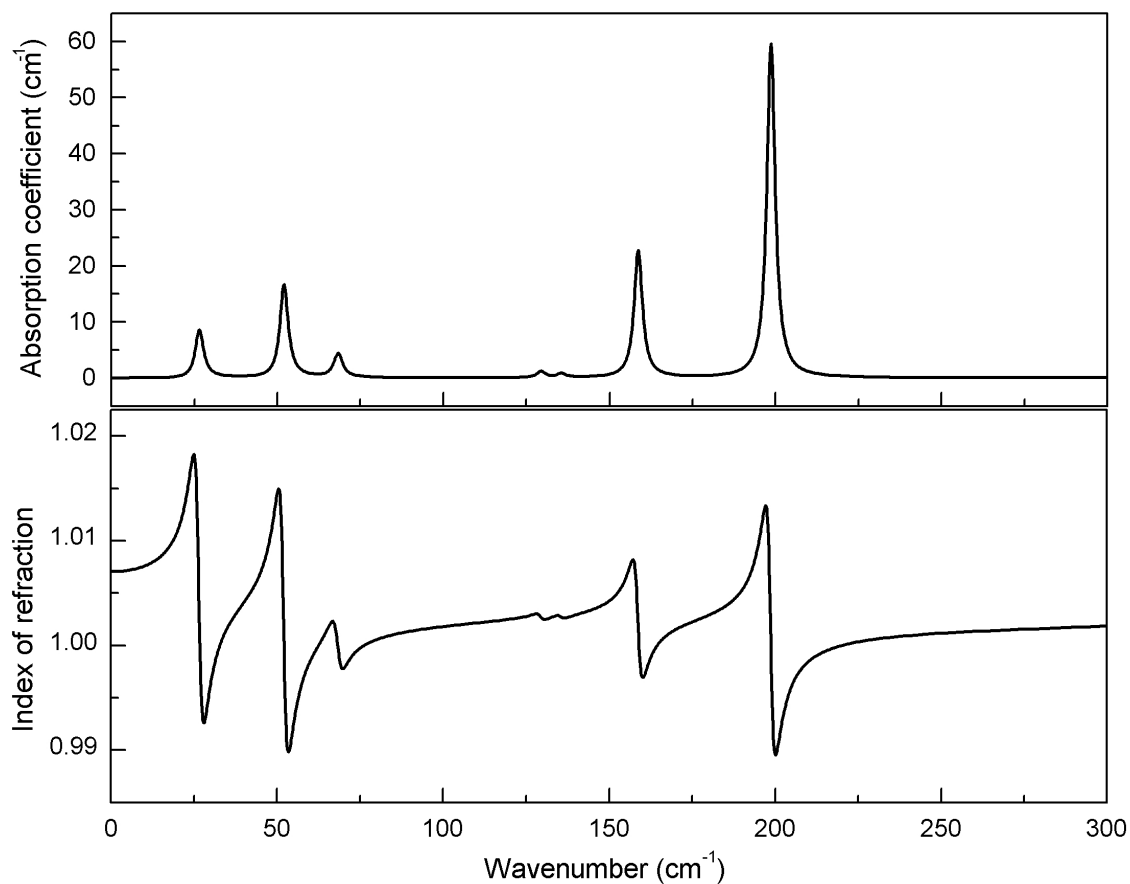

Figure A4. Absorption coefficient and index of refraction for β–HMX calculated by DFT for THz range of frequencies, where adjustable parameters $\gamma = 3$ cm^{-1} and N $= 4$ cm^{-2}.

Table A1. Modifications to S-matrix computer program presented in reference 14.

Page #	Old	New

16	if (ISCAN .eq. 0) then ! angle scan
	   write(2,*) ' ANGLE Rp Rs '
	   do I = 1,NMESHA+NBINA-1
		if (ISCAN .eq. 0) then ! angle scan
		   write(2,*) ' ANGLE Rp Rs '
		   do I = 1,NMESHA

16	write(3,*) ' ANGLE Rp Rs ' do I = 1,NMESHA	write(3,*) ' ANGLE Rp Rs ' do I = 1,NMESHA-NBINA2

16	do IB = 1,NBINA
	  ref1b=ref1b+ref1(I-NBINA2+IB-1)
	  ref2b=ref2b+ref2(I-NBINA2+IB-1)
	end do
		do IB = 1,NBINA
		  ref1b=ref1b+ref1(I-NBINA2+IB)
		  ref2b=ref2b+ref2(I-NBINA2+IB)
		end do

17	else ! frequency scan write(2,*) ' wnum frequency Rp Rs ' do J = 1,NMESHF+NBINF-1	else ! frequency scan write(2,*) ' wnum frequency Rp Rs ' do J = 1,NMESHF

17	write(3,*) ' wnum frequency Rp Rs '
	do J = 1,NMESHF
	  ref1b=0.0d0
	  ref2b=0.0d0
	  do JB = 1,NBINF
	    ref1b=ref1b+ref1(J-NBINF2+JB-1)
	    ref2b=ref2b+ref2(J-NBINF2+JB-1)
	   end do
		write(3,*) ' wnum frequency Rp Rs '
		do J = NBINF2,NMESHF-NBINF2
		  ref1b=0.0d0
		  ref2b=0.0d0
		  do JB = 1,NBINF
		    ref1b=ref1b+ref1(J-NBINF2+JB)
		    ref2b=ref2b+ref2(J-NBINF2+JB)
		   end do

References

1. P. Hohenberg and W. Kohn, "Inhomogeneous Electron Gas" Phys. Rev. **136**, B864, (1964).
2. W. Kohn and L. J. Sham, "Self-Consistent Equations Including Exchange and Correlation Effects" Phys. Rev. **140**, A1133 (1965).
3. R.O. Jones and O. Gunnarson, "The density functional formalism, its applications and prospects" Rev. Mod. Phys. **61**, 689 (1989).
4. M.R. Pederson and K.A. Jackson, Phys. Rev. B v. 41, 7453 (1990)
5. K.A. Jackson and M.R. Pederson, Phys. Rev. B v. 42, 3276 (1990)
6. A. Briley, M.R. Pederson, K.A. Jackson, D.C. Patton, and D.V. Porezag, Phys. Rev. B v. 58, 1786 (1998)
7. D.V. Porezag and M.R. Pederson, Phys. Rev. B v. 54, 7830 (1996)
8. D.V. Porezag and M.R. Pederson, Phys. Rev. A v. 60, 2840 (1999)
9. M.R. Pederson, D.V. Porezag, J. Kortus, and D.C. Patton, Phys. Status Solidi B v. 217, 197 (2000)
10. K. Jackson, M. R. Pederson, and D. Porezag, Z. Hajnal, and T. Frauenheim, Phys. Rev. B v. 55, 2549 (1997).
11. W.W. Hager and H. Zhang, "A survey of nonlinear conjugate gradient methods," Pacific J. Optim., 2, p. 35-58 (2006).
12. R. M. Martin, *Electronic Structures Basic Theory and Practical Methods*, Cambridge University Press, Cambridge 2004, p. 25.
13. C. A. D. Roeser and E. Mazur, "Light-Matter Interactions on Femtosecond Time Scale" in *Frontiers pf Optical Spectroscopy*, eds. B. Di Bartolo and O. Forte, NATO Science Series v. 168 p. 29, Kluwer Academic Publishers, Dordrecht – Norwell, 2005; C. F. Bohren and D. R. Huffman, *Absorption and Scattering of Light by Small Particles* (Wiley-VCH Verlag, Weinheim, 2004).
14. A. Shabaev, S.G. Lambrakos, N. Bernstein, V. Jacobs, D. Finkenstadt, "Initial Construction of a General Framework for Numerical Simulation of IED Detection and Remote Activation Scenarios" Naval Research Laboratory Memorandum Report, Naval Research Laboratory, Washington, DC, NRL/MR/6390-10-9260 (2010).
15. M. A. Ordal, L. L. Long, R. J. Bell, S. E. Bell, R. R. Bell, R. W. Alexander, Jr., amd C. A. Ward, "Optical properties of the metals Al, Co, Cu, Au, Fe, Pb, Ni, Pd, Pt, Ag, Ti, and W in the infrared and far infrared," Appl. Optics **22**, 1099 (1983).
16. H. J. Liebe, G. A. Hufford, and T. Manabe, "A model for the complex permittivity of water at frequencies below 1 THz," Int. J. Infrared and Millimeter Waves **12**,659 (1991).
17. H. D. Downing and D. Williams, "Optical constants of water in the infrared," J. Geophys. Res. **80**, 1656 (1975).